Optimal sizes of dielectric microspheres for cavity QED with strong coupling

J. R. Buck and H. J. Kimble
Norman Bridge Laboratory of Physics 12-33, California Institute of Technology, Pasadena, California 91125
(Received 18 October 2002; published 21 March 2003)

The whispering gallery modes (WGMs) of quartz microspheres are investigated for the purpose of strong coupling between single photons and atoms in cavity quantum electrodynamics (cavity QED). Within our current understanding of the loss mechanisms of the WGMs, the saturation photon number n_0 and critical atom number N_0 cannot be minimized simultaneously, so that an ''optimal'' sphere size is taken to be the radius for which the geometric mean $\sqrt{n_0 N_0}$, is minimized. While a general treatment is given for the dimensionless parameters used to characterize the atom-cavity system, detailed consideration is given to the D_2 transition in atomic cesium at $\lambda_0 = 852$ nm using fused-silica microspheres, for which the maximum coupling coefficient $g_a/(2\pi) \approx 750$ MHz occurs for a sphere radius $a = 3.63$ μm corresponding to the minimum for $n_0 \approx 6.06 \times 10^{-6}$. By contrast, the minimum for $N_0 \approx 9.00 \times 10^{-6}$ occurs for a sphere radius of $a = 8.12$ μm, while the optimal sphere size for which $\sqrt{n_0 N_0}$ is minimized occurs at $a = 7.83$ μm. On an experimental front, we have fabricated fused-silica microspheres with radii $a \sim 10$ μm and consistently observed quality factors $Q \geqslant 0.8 \times 10^7$. These results for the WGMs are compared with corresponding parameters achieved in Fabry-Perot cavities to demonstrate the significant potential of microspheres as a tool for cavity QED with strong coupling.

DOI: 10.1103/PhysRevA.67.033806 PACS number(s): 42.50.Ct, 42.55.Sa, 32.80.−t

I. INTRODUCTION

Motivated by the pioneering work of Braginsky and Ilchenko [1], some of the highest-quality optical resonators to date have been achieved with the whispering gallery modes (WGMs) of quartz microspheres [2,3]. Over the wavelength range 630–850 nm, quality factors $Q \approx 8 \times 10^9$ have been realized, and cavity finesse $\mathcal{F} = 2.3 \times 10^6$ demonstrated [2,3]. Such high-quality factors make the WGMs of small dielectric spheres a natural candidate for use in cavity QED [1,4–20].

While much of the work regarding quartz microspheres has centered around achieving the ultimate quality factors [2,3], the quality factor of the resonator is one of the factors that determines the suitability of the WGMs for investigations of cavity quantum electrodynamics in a regime of strong coupling. In this case, the coherent coupling coefficient g for a single atom interacting with the cavity mode must be much larger than all other dissipative rates, including the cavity decay rate κ and the rate of atomic spontaneous emission γ; namely, $g \gg (\kappa, \gamma)$. Note that $2g = \Omega$ gives the Rabi frequency associated with a single quantum of excitation shared by the atom-cavity system [21,22]. The atom-field interaction can be characterized by two important dimensionless parameters: the saturation photon number $n_0 \propto \gamma^2/g^2$ and the critical atom number $N_0 \propto \kappa\gamma/g^2$. Since these parameters correspond respectively, to the number of photons required to saturate an intracavity atom and the number of atoms required to have an appreciable effect on the intracavity field, strong coupling requires that $(n_0, N_0) \ll 1$. Ideally one would hope to minimize both of these parameters in any particular resonator. Unfortunately, within the context of our current understanding of the loss mechanisms of the WGMs [3], the critical parameters (n_0, N_0) cannot be minimized simultaneously in a microsphere.

Motivated by these considerations, in this paper we explore possible limits for the critical parameters (n_0, N_0) for the WGMs of quartz microspheres. Following the analysis of Refs. [4,5,18], we study the particular case of a single atom coupled to the *external* field of a WGM near the sphere's surface. We show that there are radii that minimize (n_0, N_0) individually, and that there is an ''optimal'' sphere size that minimizes the geometric mean, $\sqrt{n_0 \times N_0}$, of these two cavity-QED parameters and allows both parameters to be near their respective minima. We also report our progress in the fabrication of small microspheres with radii $a \sim 10$ μm, and compare our experimental results for Q with those from our theoretical analysis. Finally, we present a detailed comparison for the state of the art and future prospects for achieving strong coupling in cavity QED for both microsphere and Fabry-Perot cavities. Throughout the presentation, we attempt to develop a general formalism that can be applied to diverse systems. However, for definiteness we also present results for a particular system of some interest, namely, an individual cesium atom coupled to the WGMs of quartz microspheres.

II. MODES OF A MICROSPHERE

Solving for the mode structure of the resonances of a dielectric sphere in vacuum is a classic problem in electricity and magnetism, and the resulting field distributions have been known for some time [23]. The electric field of the TM, *electric type*, modes inside and outside a sphere of refractive index n at free-space wavelength λ_0 are respectively,

$$\vec{E}_{\rm in}(r,\theta,\phi) \propto l(l+1)\frac{j_l(kr)}{kr} P_l^m(\cos\theta) e^{im\phi}\hat{r} + \frac{[krj_l(kr)]'}{kr}\frac{\partial P_l^m(\cos\theta)}{\partial\theta} e^{im\phi}\hat{\theta} + \frac{im}{\sin\theta}\frac{[krj_l(kr)]'}{kr} P_l^m(\cos\theta) e^{im\phi}\hat{\phi} \quad (1)$$

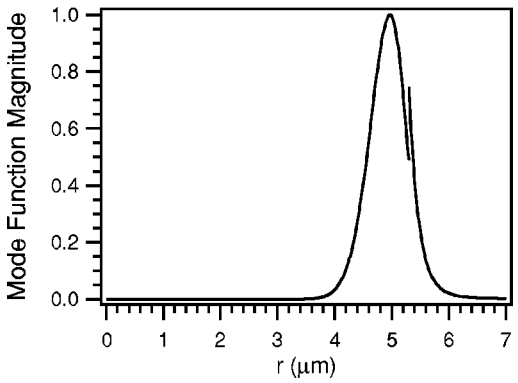

FIG. 1. The magnitude of the normalized mode function as a function of radius for the TM mode of a 5.305 μm radius sphere ($p=1, l=m=50$) with $\theta=\pi/2$ and $\phi=0$ for a wavelength of $\lambda_0 = 852.359$ nm and index of refraction $n=1.452\,46$. In our case, the function is normalized to have a maximum value of unity. Note that there is a discontinuity at the surface.

and

$$\vec{E}_{\text{out}}(r,\theta,\phi) \propto l(l+1)\frac{h_l^{(1)}\left(\frac{kr}{n}\right)}{\frac{kr}{n}}P_l^m(\cos\theta)e^{im\phi}\hat{r} + \frac{\left[\frac{kr}{n}h_l^{(1)}\left(\frac{kr}{n}\right)\right]'}{\frac{kr}{n}}\frac{\partial P_l^m(\cos\theta)}{\partial\theta}e^{im\phi}\hat{\theta} + \frac{im}{\sin\theta}\frac{\left[\frac{kr}{n}h_l^{(1)}\left(\frac{kr}{n}\right)\right]'}{\frac{kr}{n}}P_l^m(\cos\theta)e^{im\phi}\hat{\phi}, \tag{2}$$

where a is the radius of the sphere, $k=2\pi n/\lambda_0$ is the wave vector inside the sphere, $j_l(x)$ is the spherical Bessel function, $h_l^{(1)}(x)$ is the spherical Hankel function, $(\hat{r},\hat{\theta},\hat{\phi})$ are unit vectors, and the $'$ refers to differentiation with respect to the argument. Note that the TM modes have a predominantly radial electric-field vector.

In order to satisfy the boundary conditions at the surface of the microsphere, the tangential components of the mode function immediately inside and outside the sphere must be equal. However, there is a discontinuity in the radial component of the electric field at the dielectric boundary (as can be seen from Fig. 1.) The eigenmodes are determined by solving for the roots of a characteristic equation [23], which can be reduced to

$$\frac{j_{l-1}(ka)}{j_l(ka)} - \frac{nh_{l-1}^{(1)}\left(\frac{ka}{n}\right)}{h_l^{(1)}\left(\frac{ka}{n}\right)} + \frac{n^2 l}{ka} - \frac{l}{ka} = 0. \tag{3}$$

Throughout this paper, we normalize the mode functions such that their maximum value is unity. This condition then yields for the $l=m$ modes of the sphere

$$\vec{\Psi}_{\text{in}}(r,\theta,\phi) = N(l+1)\frac{j_l(kr)}{kr}\sin^l(\theta)e^{il\phi}\hat{r} + NF(r)\cos\theta\sin^{l-1}\theta e^{il\phi}\hat{\theta} + iNF(r)\sin^{l-1}\theta e^{il\phi}\hat{\phi} \tag{4}$$

and

$$\vec{\Psi}_{\text{out}}(r,\theta,\phi) = NB(l+1)\frac{h_l^{(1)}\left(\frac{kr}{n}\right)}{\frac{kr}{n}}\sin^l\theta e^{il\phi}\hat{r} + NBH(r)\cos\theta\sin^{l-1}\theta e^{il\phi}\hat{\theta} + iNBH(r)\sin^{l-1}\theta e^{il\phi}\hat{\phi}, \tag{5}$$

where

$$F(r) = \frac{j_l(kr)}{kr} + \frac{l}{2l+1}j_l(kr) - \frac{l+1}{2l+1}j_{l+1}(kr), \tag{6}$$

$$H(r) = \frac{h_l^{(1)}\left(\frac{kr}{n}\right)}{\frac{kr}{n}} + \frac{l}{2l+1}h_{l-1}^{(1)}\left(\frac{kr}{n}\right) - \frac{l+1}{2l+1}h_{l+1}^{(1)}\left(\frac{kr}{n}\right), \tag{7}$$

$$B = \frac{\frac{j_l(ka)}{ka} + \frac{l}{2l+1}j_l(ka) - \frac{l+1}{2l+1}j_{l+1}(ka)}{\frac{h_l^{(1)}\left(\frac{ka}{n}\right)}{\frac{ka}{n}} + \frac{l}{2l+1}h_{l-1}^{(1)}\left(\frac{ka}{n}\right) - \frac{l+1}{2l+1}h_{l+1}^{(1)}\left(\frac{ka}{n}\right)}, \tag{8}$$

and N is the normalization factor. Because we will require the field outside the sphere to be as large as possible, we will choose the $p=1$ modes. Also, because the coherent coupling constant $g \propto 1/\sqrt{V_{\vec{P}}}$, where $V_{\vec{P}}$ is the cavity mode volume, we choose the $l=m$ modes, since they yield the smallest electromagnetic mode volume, as will be explained in the following section.

III. ELECTROMAGNETIC MODE VOLUME

The effective mode volume $V_{\vec{P}}$ associated with the electromagnetic field distribution $\vec{\Psi}(r,\theta,\phi)$ [4] is given by

$$V_{\vec{P}} = \int_{V_Q} \varepsilon(\vec{r})|\vec{\Psi}_{\vec{P}}(\vec{r})|^2 dV, \tag{9}$$

where

$$\varepsilon(\vec{r}) = \begin{cases} n^2 & \text{if } r < a \\ 1 & \text{if } r > a \end{cases} \tag{10}$$

and $\vec{P}$ corresponds to the (p,l,m) mode. V_Q is the quantization volume discussed in Ref. [4]. As long as a radius r_Q is chosen large enough to include the effects of the evanescent field, the mode volume is relatively insensitive to the particular choice of quantization radius [24]. As discussed more extensively in Refs. [21,22] the interaction between the internal atomic degrees of freedom and the intracavity field is characterized by the coherent coupling constant $g(r,\theta,\phi)$, where

$$g(r,\theta,\phi) \equiv g_0 \vec{\Psi}^{(p,l,m)}(r,\theta,\phi) \tag{11}$$

and

$$g_0 \propto \frac{1}{\sqrt{V_{\vec{P}}}}. \tag{12}$$

Note that in the absence of damping, $2g(\vec{r})$ gives the frequency for Rabi nutation associated with a single photon in the cavity for an atom initially in the ground-state located at position $\vec{r}$ within the mode. Therefore, in order to maximize the coupling strength, one must endeavor to minimize the cavity mode volume.

In order to derive an answer that can be applied to different wavelengths, one can define a dimensionless mode volume parameter $\tilde{V}$ and plot as a function of a dimensionless sphere size parameter $\tilde{x}$ defined as

$$\tilde{V} = \frac{V_{\vec{P}}}{\left(\frac{\lambda_0}{2\pi n}\right)^3} \tag{13}$$

and

$$\tilde{x} = \frac{2\pi n a}{\lambda_0}, \tag{14}$$

where $V_{\vec{P}}$ is the cavity mode volume, n is the index of refraction at the free-space wavelength λ_0, and a is the sphere radius. The plots then only depend on the index of refraction (see Fig. 2).

Naively, one might assume that the sphere should be made as small as possible in order to minimize the electromagnetic mode volume, and hence to provide a maximum for g_0 and hence globally for $g(\vec{r})$. However, as shown in Figs. 2 and 3, the mode volume for the TM modes of a quartz microsphere actually passes through a minimum at some particular radius a_0. This behavior can be understood by noting that for $a < a_0$, the intrinsic, radiative losses are increasing rapidly and ultimately cause the mode to no longer be well confined by the sphere, with a concomitant increase of the mode volume. Note that in Fig. 2 and subsequent figures, we give results for $n \sim 1.45$ corresponding to fused silica, as well as for $n = 2.00$ and $n = 3.00$. These latter cases serve to illuminate the role of n as well as being applicable to other materials (i.e., the index of refraction for GaAs is $n = 3.4$ for $\lambda = 1550$ nm [25]). For a very low-OH fused silica microsphere at $\lambda_0 = 852$ nm (the wavelength of the D_2 transition in atomic cesium) with index of refraction $n = 1.452\,46$, the minimum mode volume $V_{\vec{P}}^{\min} \approx 28.4\ \mu\text{m}^3$ occurs for radius $a \approx 3.73\ \mu$m corresponding to mode numbers $p = 1, l = m = 34$ (see Fig. 3). One might at first believe that this value for the radius represents the optimal sphere size for use as a cavity with single atoms. However, while the mode volume $V_{\vec{P}}$ plays an important role in determining the coupling constant [Eq. (12)], it is not the only parameter relevant

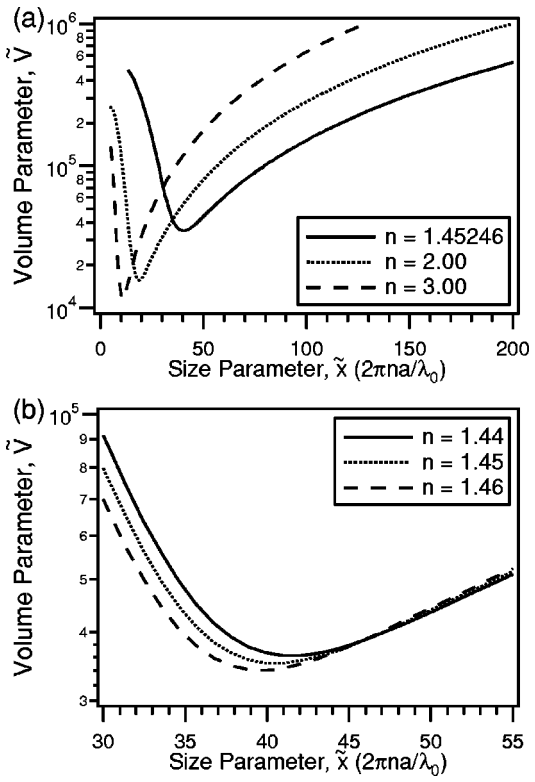

FIG. 2. (a) The dimensionless volume parameter $\tilde{V}$ [defined by Eq. (13)], as a function of the dimensionless size parameter $\tilde{x}$ [defined by Eq. (14)]. The solid line is for an index of refraction $n = 1.452\,46$, the index of refraction for fused silica at $\lambda_0 = 852$ nm, with a minimum of $\tilde{V} = 34\,883.4$ for $\tilde{x} = 39.946\,9$ ($l = m = 34$). The dotted line is for an index of refraction $n = 2.00$, with a minimum of $\tilde{V} = 15\,596.2$ for $\tilde{x} = 18.986\,4$ ($l = m = 14$). The dashed line is for an index of refraction $n = 3.00$, with a minimum of $\tilde{V} = 11\,546.4$ for $\tilde{x} = 10.274\,8$ ($l = m = 6$). (b) Because the index of refraction for fused silica varies from $n = 1.444$ at $\lambda_0 = 1550$ nm to $n = 1.458$ for $\lambda_0 = 600$ nm (see Fig. 4), this plot of the dimensionless volume parameter $\tilde{V}$ as a function of the dimensionless size parameter $\tilde{x}$ is made for that range of values. The solid line is for an index of refraction $n = 1.44$, with a minimum of $\tilde{V} = 36\,247.5$ for $\tilde{x} = 40.981\,2$, ($l = m = 35$). The dotted line is for an index of refraction $n = 1.45$, with a minimum of $\tilde{V} = 35\,161.1$ for $\tilde{x} = 41.003\,6$, ($l = m = 35$). The dashed line is for an index of refraction $n = 1.46$, with a minimum of $\tilde{V} = 34\,129.1$ for $\tilde{x} = 39.963\,1$, ($l = m = 34$).

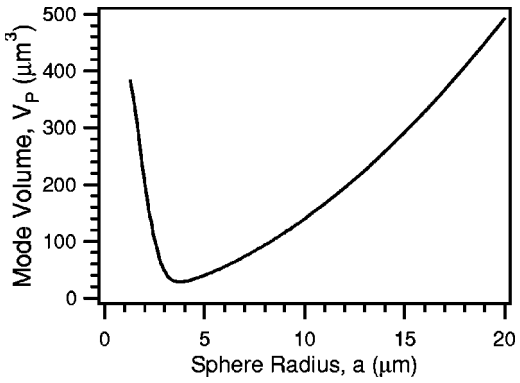

FIG. 3. The electromagnetic mode volume $V_{\vec{P}}$ for the TM modes of a very low-OH fused silica microsphere as a function of sphere radius at the wavelength $\lambda_0 = 852$ nm for the D_2 line of atomic cesium. The minimum, 28.4 μm^3, occurs for radius $a_0 \approx 3.73$ μm corresponding to mode numbers $p=1$ and $l=m=34$.

to cavity QED with single atoms in a regime of strong coupling. As discussed in the following sections, the quality factor Q of a WGM has a strong dependence on the sphere radius, and must also be considered in an attempt to optimize the critical atom and saturation photon numbers.

IV. LOSSES IN DIELECTRIC SPHERES

For fused silica spheres with radius $a \gtrsim 15$ μm, the effect of intrinsic radiative losses can be safely neglected, since they allow quality factor $Q \gtrsim 10^{21}$, as illustrated in Fig. 5. Such large values of Q greatly exceed those imposed by technical constraints of material properties, such as bulk absorption and surface scattering.

However, as one moves to very small spheres with radius $a \lesssim 10$ μm, the intrinsic radiative Q falls steeply enough to become the dominant loss mechanism even in the face of other technical imperfections. When assessing the usefulness of microspheres for cavity QED, one must account for the entire set of loss mechanisms to determine the optimal size for the microsphere, which is the subject to which we now turn our attention.

The quality factors of the WGMs of fused silica microspheres are determined by several different loss mechanisms.

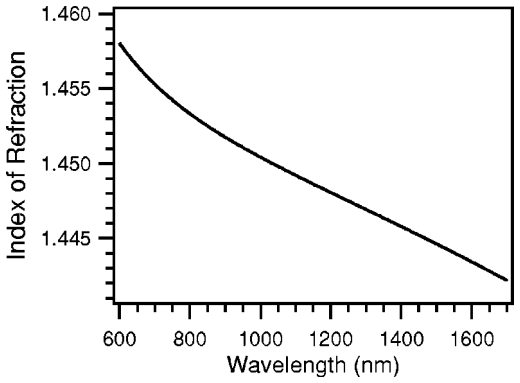

FIG. 4. The index of refraction of very low-OH fused silica as a function of wavelength.

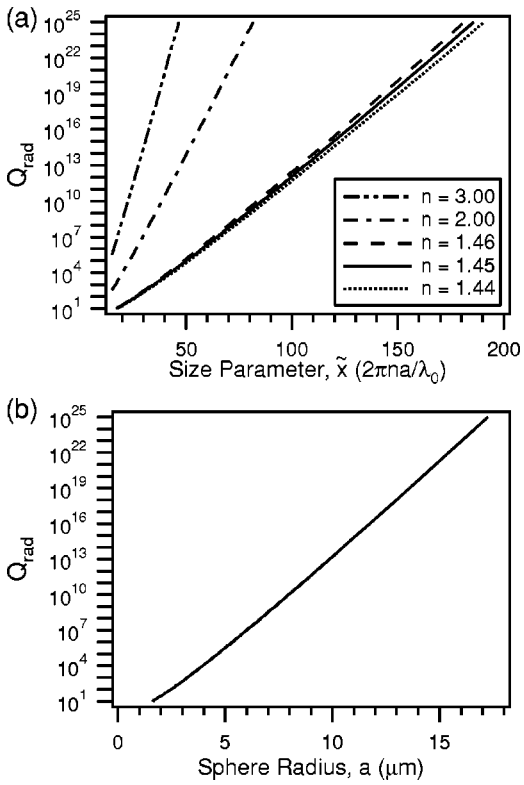

FIG. 5. (a) Semi-log plot of the radiative quality factor $Q_{\rm rad}$ for various indices of refraction as a function of the dimensionless size parameter $\tilde{x} = 2\pi na/\lambda_0$. (b) Semi-log plot of the radiative quality factor $Q_{\rm rad}$ as a function of sphere radius for a wavelength of $\lambda_0 = 852.359$ nm (index of refraction is $n = 1.452\,46$).

The overall quality factor can then be calculated by adding the different contributions in the following way [2]:

$$Q^{-1} = Q_{\rm rad}^{-1} + Q_{\rm mat}^{-1}, \tag{15}$$

$$Q_{\rm mat}^{-1} = Q_{\rm s.s.}^{-1} + Q_{\rm w}^{-1} + Q_{\rm bulk}^{-1}, \tag{16}$$

where $Q_{\rm rad}$ is due to purely radiative losses for an ideal dielectric sphere and $Q_{\rm mat}$ results from nonideal material properties. The principal mechanisms contributing to $Q_{\rm mat}$ are scattering losses from residual surface inhomogeneities ($Q_{\rm s.s.}$), absorption losses due to water on the surface of the sphere ($Q_{\rm w}$), and bulk absorption in the fused silica ($Q_{\rm bulk}$). The intrinsic material losses are known very accurately, since they arise from absorption in the material at the wavelength of concern [26]. Considerably greater uncertainty is associated with the losses due to surface scattering and absorption due to adsorbed material on the surface of the sphere, of which water is likely the principal component. We will adopt the models for these losses presented in Refs. [2,3], extrapolated to the regime of small spheres of interest here.

A. Intrinsic radiative losses

The contribution to the quality factor for purely radiative effects $Q_{\rm rad}$ can be derived by following the arguments presented in Ref. [27]. These losses are due to the leakage of light from the resonator due to its finite dielectric constant

and radius of curvature. The results can then be compared to numerical results obtained by Lorenz-Mie theory [28]. We find from Ref. [27] that

$$Q_{\mathrm{rad}}=\frac{1}{2}\left(l+\frac{1}{2}\right)n^{1-2b}(n^2-1)^{1/2}e^{2T_l}, \tag{17}$$

where

$$T_l=\left(l+\frac{1}{2}\right)(\eta_l-\tanh\eta_l), \tag{18}$$

$$\eta_l=\operatorname{arccosh}\left\{n\left[1-\frac{1}{l+\frac{1}{2}}\left(t_p^0\xi+\frac{l^{1-2b}}{\sqrt{l^2-1}}\right)\right]^{-1}\right\}, \tag{19}$$

$$\xi=\left[\frac{1}{2}\left(l+\frac{1}{2}\right)\right]^{1/3}, \tag{20}$$

and

$$b=\begin{cases}0 & \text{TE modes}\\ 1 & \text{TM modes.}\end{cases} \tag{21}$$

Also, n is the index of refraction and t_p^0 is the pth zero of the Airy function Ai. This p corresponds to the mode number (p,l,m). In our case, we are only interested in the $p=1$ modes of the sphere to maximize the electromagnetic field outside the sphere while maintaining a small mode volume. Note that these expressions for Q_{rad} become invalid in the limit of small l mode numbers. The error in the mode functions used to derive these results reaches 1% for $l=18$. However, the error is less than 0.2% for $l=76$ (This is the optimal sphere size discussed in Sec. VI). Fortunately, the expressions are valid in the regimes for which we are concerned. This has been confirmed by making comparisons with numerical values obtained using Lorenz-Mie scattering theory.

From Fig. 5, we see that the radiative Q falls approximately exponentially as the radius a is decreased, and can become quite important as the sphere size is decreased below 10 μm. For example, for a 15 μm radius sphere and a wavelength $\lambda_0=852.359$ nm, $Q_{\mathrm{rad}}\approx 2\times 10^{21}$. Therefore, the net quality factor would most certainly be dominated by other loss mechanisms in Eq. (15). However, for a 7 μm radius sphere, $Q_{\mathrm{rad}}\approx 4\times 10^{8}$, and the radiative losses can play a crucial role in the characteristics of the spheres that are optimal for use in cavity QED.

B. Material loss mechanisms

The quality factor due to bulk absorption Q_{bulk} in fused silica is actually known very well, since this depends only on the absorption of the material at the wavelength of concern [2]:

$$Q_{\mathrm{bulk}}=\frac{2\pi n}{\alpha\lambda_0}, \tag{22}$$

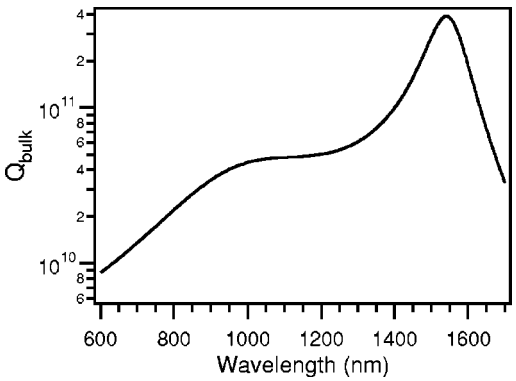

FIG. 6. The quality factor, Q_{bulk}, from Eq. (22) for a very low-OH fused silica microsphere as a function of wavelength. Because fused silica has a minimum in absorption at 1550 nm, there is a maximum for the quality factor due to bulk absorption of $Q_{\mathrm{bulk}}\sim 3.8\times 10^{11}$. At 852 nm, the quality factor due to bulk absorption is $Q_{\mathrm{bulk}}\sim 2.4\times 10^{10}$.

where n is the index of refraction, and α is the absorption coefficient of the material. From Fig. 6 we see that for very low-OH fused silica, the absorption coefficient at 852 nm is $\alpha\approx 4.5\times 10^{-4}$ m^{-1} [26]. This would correspond to a quality factor of $Q_{\mathrm{bulk}}\sim 2.4\times 10^{10}$. Fused silica has a minimum in its absorption coefficient of $\alpha\approx 1.5\times 10^{-5}$ m^{-1} at 1550 nm, which yields a quality factor of $Q_{\mathrm{bulk}}\sim 3.8\times 10^{11}$.

The quality factor due to surface scattering $Q_{\mathrm{s.s.}}$ and absorption by adsorbed water Q_{w} has also been studied and modeled, Albeit for larger spheres with $a\gtrsim 600$ μm. For losses due to surface scattering, we follow the work of Refs. [2,3] and take

$$Q_{\mathrm{s.s.}}\sim\frac{3\varepsilon(\varepsilon+2)^2}{(4\pi)^3(\varepsilon-1)^{5/2}}\frac{\lambda_0^{7/2}(2a)^{1/2}}{(\sigma B)^2}, \tag{23}$$

where $\varepsilon=n^2$ is the dielectric constant and $\sigma B\sim 5$ nm^2 is an empirical parameter determined by the size and correlation length of the distribution of residual surface inhomogeneities. This quantity was reported in Ref. [3] based upon atomic force microscopy measurements of a microsphere.

The quality factor due to water adsorbed on the surface, Q_{w}, is given by [3]

$$Q_{\mathrm{w}}\sim\sqrt{\frac{\pi}{8n^3}}\frac{(2a)^{1/2}}{\delta\lambda_0^{1/2}\beta_w}, \tag{24}$$

where $\delta\sim 0.2$ nm is an estimated thickness for the water layer, and $\beta_w\sim 4.33$ m^{-1} is the absorption coefficient of water at 852 nm.

Combining these various results, we display in Fig. 7 a curve for the quantity Q_{mat} as a function of sphere radius a for a wavelength $\lambda_0=852$ nm. This same figure shows the quality factor Q_{rad}, set by intrinsic radiative losses [Eq. (17)], as well as the overall quality factor $Q=Q_{\mathrm{rad}}Q_{\mathrm{mat}}/(Q_{\mathrm{rad}}+Q_{\mathrm{mat}})$. From this plot, we see that the radiative losses dominate the overall quality factor below a radius of $a\lesssim 8$ μm, while the losses due to material proper-

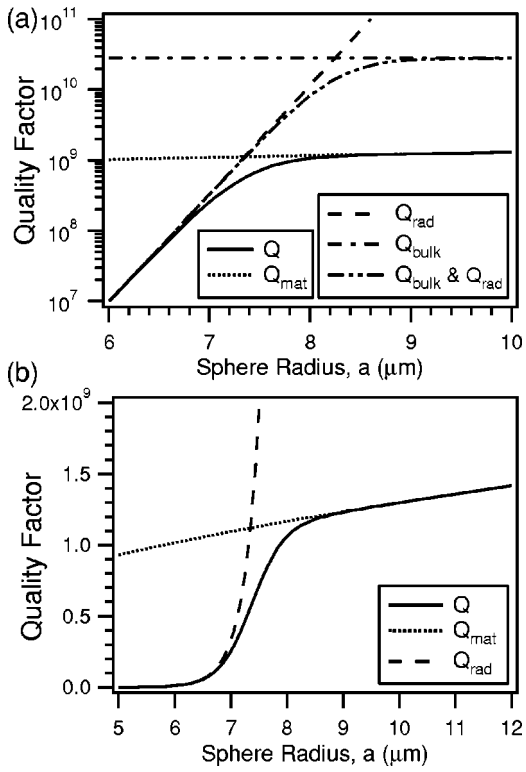

FIG. 7. (a) Semilog plot of the quality factors due to the various loss mechanisms discussed in Sec. IV for a very low-OH fused silica microsphere as a function of sphere radius for the $l=m$, TM modes at a wavelength of $\lambda_0=852$ nm. In particular, traces are shown for the quality factor due to purely radiative losses (Q_{rad}), the bulk absorption of fused silica (Q_{bulk}), both radiative losses and bulk absorption, the three loss mechanisms comprising Q_{mat}: ($Q_{\mathrm{bulk}}, Q_{\mathrm{s.s.}}, Q_{\mathrm{w}}$), and the predicted Q due to all four loss mechanisms. (b) This linear plot zooms in on the region of interest at the transition where the radiative losses become the dominant loss mechanism. The plot contains the quality factor due to purely radiative losses (Q_{rad}), the three loss mechanisms comprising Q_{mat}: ($Q_{\mathrm{bulk}}, Q_{\mathrm{s.s.}}, Q_{\mathrm{w}}$), and the predicted Q due to all four loss mechanisms.

ties are most significant for $a \gtrsim 8\ \mu$m. Because of the extremely steep dependence of Q_{rad} on sphere size, the point of transition from material to radiative dominated loss should be reasonably insensitive to details of the models employed to describe the material losses. Although we focus our attention here on the wavelength appropriate to the particular case of the D_2 transition in atomic cesium, a similar analysis could be carried out for other wavelengths of interest using the above formalism, as for example the $2S \rightarrow 2P$ transition at 1.083 μm in metastable helium.

V. THE STRONG COUPLING REGIME

The ultimate goal that we consider here is to employ the WGMs of quartz microspheres as cavity modes for achieving strong coupling to atoms within the setting of cavity QED. The atom of choice in this paper is cesium, and in particular, the D_2 $(F=4 \mapsto F'=5)$ transition in cesium at $\lambda_0 = 852.359$ nm as an illustrative example. Such an analysis allows a direct comparison with the state of the art in Fabry-Perot cavities [29].

The coupling coefficient $g(\vec{r})$ is the coupling frequency of a single atom to a particular cavity mode and corresponds to one-half the single-photon Rabi frequency [21,22]. For an atom located just at the outer surface of the microsphere (i.e., in vacuum) and interacting with a whispering gallery mode $\vec{P}=(p,l,m)$, the coupling coefficient is given by [4]

$$g(a) \equiv g_a = \gamma_\perp |\vec{\Psi}_{\mathrm{out}}(a)| \sqrt{\frac{V_0}{V_{\vec{P}}}}, \tag{25}$$

where a is the sphere radius, $\gamma_\perp/2\pi = 2.61$ MHz is the transverse spontaneous decay rate for our transition in cesium, $V_0 = 3c\lambda_0^2/4\pi\gamma_\perp$ is the effective volume of the atom for purely radiative interactions, and $V_{\vec{P}}$ is the electromagnetic mode volume of the whispering gallery mode designated by $\vec{P}=(p,l,m)$.

Armed with a knowledge of g, we are now able to determine certain dimensionless parameters relevant to the strong coupling regime of cavity QED. In particular, we consider an atom-cavity system to be in the strong coupling regime when the single-photon Rabi frequency $2g$ for a single intracavity atom dominates the cavity field decay rate κ the atomic dipole decay rate $\gamma_\perp$ and the inverse atomic transit time T^{-1} [21,22]. We will defer further discussion of T^{-1}, however, this requirement relates to the need for atomic localization [4,5]. In the strong coupling regime, important parameters for characterizing the atom-cavity system are the two dimensionless parameters: the saturation photon number n_0, and the critical atom number N_0. The saturation photon number, given by

$$n_0 \equiv \frac{\gamma_\perp^2}{2g^2}, \tag{26}$$

corresponds to the number of photons required to saturate an intracavity atom [21,22]. The critical atom number, defined by

$$N_0 \equiv \frac{2\gamma_\perp \kappa}{g^2}, \tag{27}$$

corresponds to the number of atoms required to have an appreciable effect on the intracavity field [21,22]. Ideally, one hopes to minimize simultaneously both the critical atom number N_0 and the saturation photon number n_0 which corresponds to simultaneous maxima for both $g^2/\kappa\gamma_\perp$ and $g^2/\gamma_\perp^2$.

The saturation photon number and critical atom number are useful because of their physical meaning. However, one can define a new dimensionless parameter

$$\beta = \frac{8\pi^2 V_{\vec{P}}}{3\lambda_0^3} \frac{1}{|\vec{\Psi}_{\mathrm{out}}(a)|^2}, \tag{28}$$

that corresponds to the cavity mode volume in units of λ^3 weighted by the inverse of the strength of the mode function at the atomic position. This enables the equations for the saturation photon number and critical atom number to be expressed as

$$n_0 = \frac{\beta}{4Q_{\text{atom}}} \tag{29}$$

and

$$N_0 = \frac{\beta}{Q_{\text{cavity}}}, \tag{30}$$

where

$$Q_{\text{atom}} = \frac{\pi c}{\lambda_0 \gamma_\perp} \tag{31}$$

and

$$Q_{\text{cavity}} = \frac{\pi c}{\lambda_0 \kappa}. \tag{32}$$

This parameter β then also determines the coupling coefficient in the following manner:

$$g(a) = \sqrt{\frac{2\pi c \gamma_\perp}{\beta \lambda_0}}. \tag{33}$$

Therefore, we see that one can use a single parameter β combined with the properties of the atom to be used (λ_0 and $\gamma_\perp$) and the quality factor of the resonator, Q_{cavity}, to determine the three parameters (n_0, N_0, g_0) of importance in determining the quality of an atom-cavity system.

Figures 8 and 9 are plots of this dimensionless parameter β and of $1/\sqrt{\beta}$ as functions of the dimensionless size parameter $\tilde{x} = 2\pi na/\lambda_0$ for a few values of index of refraction. Because the index of refraction for fused silica varies from $n = 1.444$ at $\lambda_0 = 1550$ nm to $n = 1.458$ for $\lambda_0 = 600$ nm (see Fig. 4), Figs. 8(b) and 9(b) are made for that range of values. From Figs. 8 and 9 one sees that there is a minimum for β and a maximum for $1/\sqrt{\beta}$ that depends on the index of refraction.

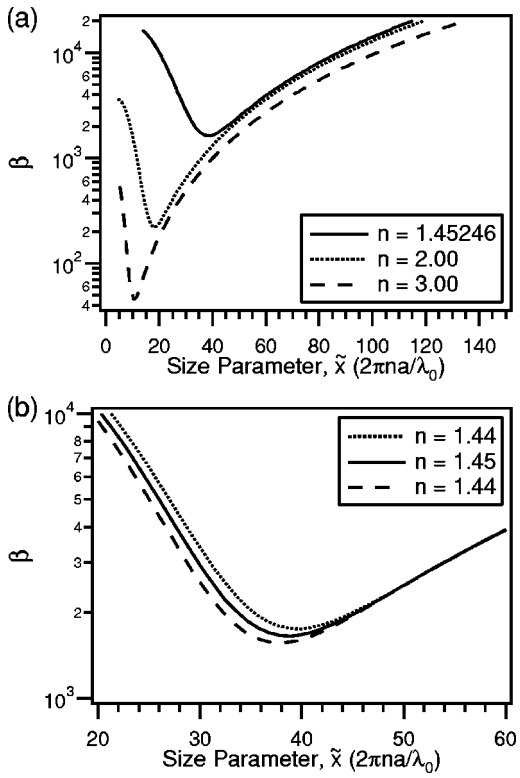

FIG. 8. (a) The dimensionless parameter β as a function of the dimensionless size parameter $\tilde{x} = 2\pi na/\lambda_0$. For an index of refraction $n = 1.452\,46$ (i.e., the index of refraction for fused silica at $\lambda_0 = 852$ nm), there is a minimum of $\beta = 1\,632.01$ for $\tilde{x} = 38.883\,3$, $(l = m = 33)$. For an index of refraction $n = 2.00$, there is a minimum of $\beta = 221.124$ for $\tilde{x} = 17.876\,3$, $(l = m = 13)$. For an index of refraction $n = 3.00$, there is a minimum of $\beta = 45.374\,4$ for $\tilde{x} = 10.274\,8$, $(l = m = 6)$. (b) Because the index of refraction for fused silica varies from $n = 1.444$ at $\lambda_0 = 1550$ nm to $n = 1.458$ for $\lambda_0 = 600$ nm (see Fig. 4), this plot is made for that range of values. For an index of refraction $n = 1.44$, there is a minimum of $\beta = 1\,753.92$ for $\tilde{x} = 39.918\,8$, $(l = m = 34)$. For an index of refraction $n = 1.45$, there is a minimum of $\beta = 1\,653.7$ for $\tilde{x} = 38.877\,8$, $(l = m = 33)$. For an index of refraction $n = 1.46$, there is a minimum of $\beta = 1\,561.45$ for $\tilde{x} = 37.834\,8$, $(l = m = 32)$.

VI. STRONG COUPLING WITH CESIUM

The results of the previous section can now be used to determine the saturation photon number n_0 the critical atom number N_0 and the coupling coefficient $g(a)$ for any atomic transition. In our case, we are concerned with the D_2 transition in cesium ($\lambda_0 = 852.359$ nm). For this transition, the spontaneous transverse decay rate is $\gamma/2\pi = 2.61$ MHz. Also, at this wavelength the index of refraction for fused silica is $n = 1.452\,46$. This allows one to compute the coupling coefficient, $g(a) = \sqrt{2\pi c \gamma_\perp / \beta \lambda_0}$. Figure 10 shows that there is a maximum of $g/2\pi = 749.986$ MHz for a radius $a = 3.63$ μm, $(l = m = 33)$. Interestingly, because we are restricted to having the atom couple to the *external* field of the microsphere, the maximum in the coupling coefficient $g(a)$ does not coincide with the minimum for the mode volume, $V_{\tilde{P}}$ (see Figs. 3 and 10.)

The saturation photon number n_0 is proportional to the dimensionless parameter β as shown in Eq. (29). Since the factor of proportionality is a constant that depends only on the properties of the particular atom of concern, the curve is determined by that of β along with the quality factor of the atomic resonance (in our case cesium), which is given by Eq. (31) to be $Q_{atom} = 6.738 \times 10^7$. Figure 11 is a plot of the saturation photon number for the D_2 transition in cesium as a function of sphere size. Figure 11 shows that there is a minimum for the saturation photon number of $n_0 = 6.055\,27 \times 10^{-6}$ for a sphere radius of $a = 3.631\,63$ μm $(l = m = 33)$.

The critical atom number N_0 is also proportional to the dimensionless parameter β as shown in Eq. (30). However,

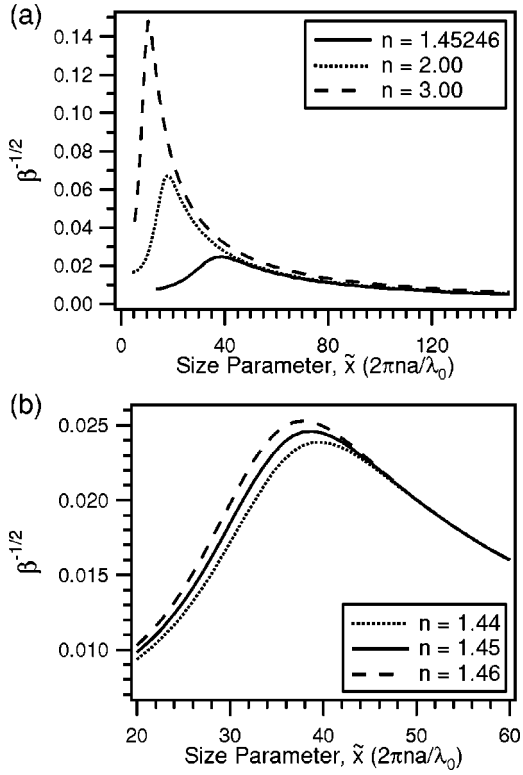

FIG. 9. (a) The dimensionless parameter $1/\sqrt{\beta}$ as a function of the dimensionless size parameter $\tilde{x}=2\pi na/\lambda_0$. For an index of refraction $n=1.452\,46$ (i.e., the index of refraction for fused silica at $\lambda_0=852$ nm), there is a maximum of $1/\sqrt{\beta}=0.024\,753\,6$ for $\tilde{x}=38.883\,3$, $(l=m=33)$. For an index of refraction $n=2.00$, there is a maximum of $1/\sqrt{\beta}=0.067\,248\,4$ for $\tilde{x}=17.876\,3$, $(l=m=13)$. For an index of refraction $n=3.00$, there is a maximum of $1/\sqrt{\beta}=0.148\,455$ for $\tilde{x}=10.274\,8$, $(l=m=6)$. (b) Because the index of refraction for fused silica varies from $n=1.444$ at $\lambda_0=1550$ nm to $n=1.458$ for $\lambda_0=600$ nm (see Fig. 4), this plot is made for that range of values. For an index of refraction $n=1.44$, there is a maximum of $1/\sqrt{\beta}=0.023\,877\,9$ for $\tilde{x}=39.918\,8$, $(l=m=34)$. For an index of refraction $n=1.45$, there is a minimum of $1/\sqrt{\beta}=0.024\,590\,8$ for $\tilde{x}=38.877\,8$, $(l=m=33)$. For an index of refraction $n=1.46$, there is a minimum of $1/\sqrt{\beta}=0.025\,306\,8$ for $\tilde{x}=37.834\,8$, $(l=m=32)$.

its factor of proportionality is the quality factor of the resonator, Q_{cavity}, which has a very strong dependence on the sphere radius a in the region below 10 μm (see Fig. 7). Therefore, the minimum for the critical atom number does not occur for the same sphere size as for the saturation photon number. Figure 12 is a plot of the critical atom number as a function of sphere size. Using for Q_{cavity} the model that incorporates all of the loss mechanisms discussed in Sec. IV (radiative losses, bulk absorption, surface scattering, and absorption due to water on the surface), we find that the minimum for the critical atom number $N_0=8.999\,35\times10^{-6}$ occurs for a sphere radius of $a=8.12015$ μm $(l=m=79)$. At this radius, the coupling coefficient is $g/(2\pi)=304.16$ MHz.

Unfortunately, as illustrated in Fig. 13, the minima for the two parameters, n_0 and N_0, do not occur for the same sphere radius. However, if one uses the minimum of the geometric mean of the two parameters, each can have a value near its respective minimum. The minimum of the geometric mean occurs for a sphere radius $a=7.830\,38$ μm $(l=m=76)$. For this sphere size, the coupling coefficient is $g/2\pi=318.333$ MHz, the saturation photon number is $n_0=3.361\,07\times10^{-5}$, and the critical atom number is $N_0=9.278\,34\times10^{-6}$. Therefore, each cavity QED parameter can be made to achieve simultaneously a value near its respective minimum.

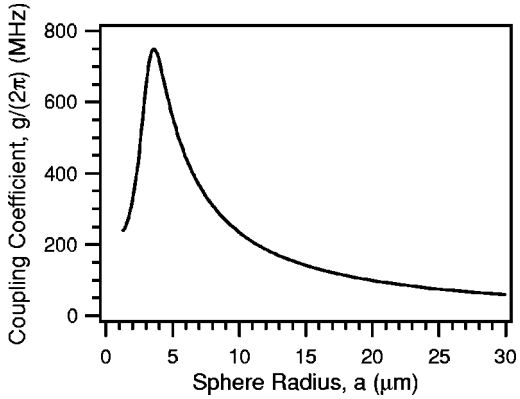

FIG. 10. The coupling coefficient, $g/2\pi$, as a function of sphere size for the D_2 transition in cesium ($\lambda_0=852.359$ nm). There is a maximum of $g/2\pi=749.986$ MHz for a sphere radius of $a=3.631\,63$ μm, $(l=m=33)$. Note that the maximum for $g/2\pi$ does not coincide with the minimum for the cavity mode volume, $V_{\vec{P}}$ (see Fig. 3).

VII. PROGRESS IN SMALL SPHERE MANUFACTURE

A large portion of the work being done on microspheres has been to push the quality factors of the spheres to record levels [2,3]. This effort has produced some of the highest finesse ($\mathcal{F}=2.3\times10^6$) optical cavities to date with quality factors $Q\sim10^{10}$ [2,3]. However, we have seen that Q is not the only relevant factor in determining the suitability of the WGMs for cavity QED in a regime of strong coupling. In

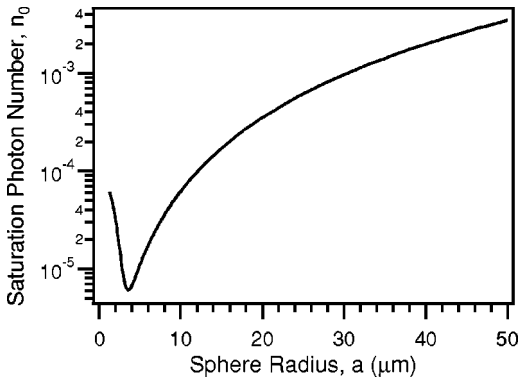

FIG. 11. The saturation photon number n_0 as a function of sphere size for the D_2 transition in cesium ($\lambda_0=852.359$ MHz). There is a minimum $n_0=6.055\,27\times10^{-6}$ for a sphere radius of $a=3.631\,63$ μm $(l=m=33)$. At this radius, the coupling coefficient is $g/2\pi=749.986$ MHz.

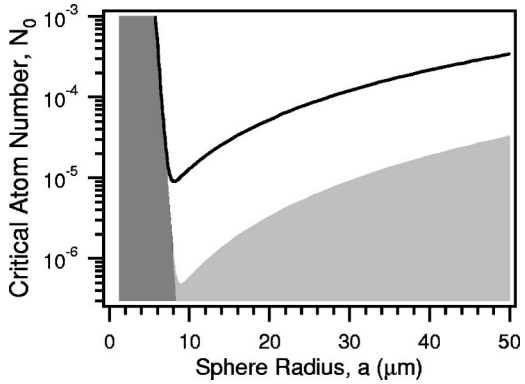

FIG. 12. The critical atom number N_0 as a function of sphere size for the D_2 transition in cesium ($\lambda_0 = 852.359$ MHz). There is a minimum $N_0 = 8.999\,35 \times 10^{-6}$ for a sphere radius of $a = 8.1201\,5$ μm ($l = m = 79$). At this radius, the coupling coefficient is $g/2\pi = 304.16$ MHz. This plot of the critical atom number incorporates the model for the quality factor of the resonator, Q_{cavity}, outlined in Sec. IV, for the four loss mechanisms: bulk absorption, surface scattering, absorption due to water on the surface, and radiative losses. The dark gray region is bounded by the effects of purely radiative losses. The light gray region is bounded by the effects of both radiative losses and bulk absorption.

general, the preceding analysis demonstrates the requirement to push to microspheres of small radius, $a \lesssim 10$ μm. Unfortunately, the experiments that have achieved the highest quality factors and which have investigated certain material loss mechanisms are of rather larger size, and hence not optimal for cavity QED in a regime of strong coupling. For example, the experiment of Ref. [3] achieved a quality factor of $Q = 7.2 \times 10^9$ at 850 nm in a sphere of radius $a = 340$ μm.

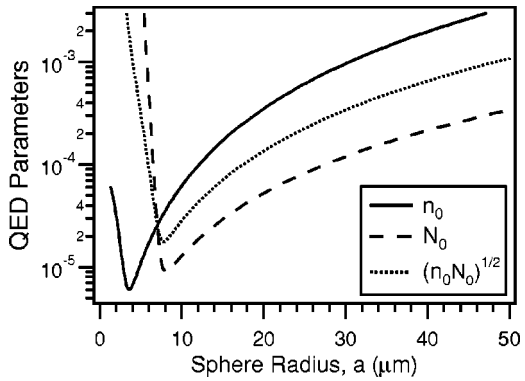

FIG. 13. This plot shows the two parameters, (n_0, N_0), of importance to cavity QED as a function of sphere radius. The geometric mean of these two parameters is also plotted. The solid line represents the saturation photon number n_0, the dashed line gives the critical atom number N_0, and the dotted line shows the geometric mean of the two parameters, $\sqrt{n_0 N_0}$. The minimum of each plot corresponds to the following dimensionless parameters: $n_0 = 6.05527 \times 10^{-6}$ for $a = 3.631\,63$ μm ($l = m = 33$), and $N_0 = 8.999\,35 \times 10^{-6}$ at $a = 8.120\,15$ μm ($l = m = 79$). The two curves cross at $a = 7.03$ μm with $n_0 = N_0 = 2.56 \times 10^{-5}$. The geometric mean of these two parameters, $\sqrt{n_0 \times N_0}$, is minimized for $a = 7.830\,38$ μm ($l = m = 76$). For this radius, the parameters are: $n_0 = 3.361\,07 \times 10^{-5}$ and $N_0 = 9.278\,34 \times 10^{-6}$. Note that the curve for N_0 assumes the model for the Q discussed in this paper, and that the coupling coefficient $g(\vec{r})$ is evaluated at the maximum of the mode function for $r = a$.

To explore the possibilities of cavity QED with strong coupling in substantially smaller spheres, we have undertaken a program to study fabrication techniques for quartz microspheres with $a \lesssim 30$ μm, while still maintaining high-quality factors. We have been able to fabricate 10 μm radius spheres using an oxygen-hydrogen microtorch to melt the ends of very low-OH fused silica rods to form a sphere on the end of a stem. Light is then coupled to the sphere using frustrated total internal reflection of a prism, as in Refs. [3,4,31]. Our observations demonstrate that spheres of this size can be made consistently to have quality factors $Q \gtrsim 0.8 \times 10^7$. While this is encouraging progress, the resulting Q is two orders of magnitude smaller than the theoretical maximum of $\approx 1.3 \times 10^9$ for this size based upon the model discussed in Sec. IV.

One possible reason for this discrepancy could be the importance of minimizing the ellipticity of the small spheres. Because the small resonators fabricated by our technique have a stem protruding out of them, they are far from spherical. When coupling to an $l = m$ mode in spheres with $a \gtrsim 100$ μm and hence large l, the mode is tightly confined to the equator; therefore, the poles do not have an appreciable impact on the mode structure or quality factor. In this case, it is not of critical importance to have the best sphere possible, but rather the best great circle possible to achieve large quality factors. However, this is not the case in small spheres with $a \lesssim 10$ μm. As a decreases, the $l = m$ modes occupy an increasingly larger proportion of the sphere in polar angle, and the ellipticity of the sphere becomes increasingly important in determining the mode structure as well as the Q. However, while there is certainly room for improvement in our fabrication technique and in the resulting mode structures and quality factors, we shall see in the following section that the current results have promising implications.

VIII. COMPARING MICROSPHERES AND FABRY-PEROT CAVITIES

Figure 14 offers a comparison of the state of the art for Fabry-Perot and microsphere cavities for cavity QED, as well as projections of likely limits for each. It is interesting to note that in our projections for the limiting cases of each, microspheres allow for a significant improvement in the critical atom number N_0 relative to Fabry-Perot cavities. On the other hand, a principal advantage of Fabry-Perot cavities relative to microspheres would seem to be significant improvements in the saturation photon number n_0. The specific specific task at hand would then dictate which technology to apply.

As shown in Fig. 14, there has already been some progress in coupling atoms to the external fields of a microsphere [31]. The sphere employed for the work of Ref. [31] had a radius of $a \approx 60$ μm, and quality factor $Q \lesssim 5 \times 10^7$, corresponding to a mode volume of $V_{\vec{P}} \approx 3.7 \times 10^3$ μm^3, coupling coefficient $g_a/(2\pi) \approx 24$ MHz, saturation photon

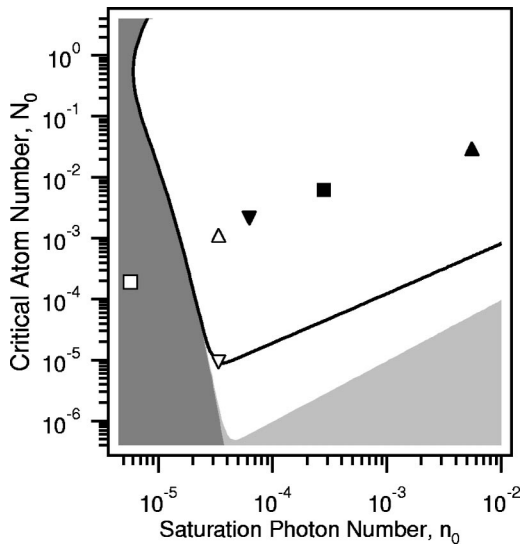

FIG. 14. The solid line gives a parametric plot of the critical atom number N_0 and the saturation photon number n_0, for fused-silica microspheres and the D_2 transition of atomic cesium, incorporating the loss mechanisms outlined in Sec. IV. The dark gray region is bounded by the effects of radiative losses. The light gray region is bounded by the effects of bulk absorption and radiative losses. This plot also offers a comparison of experimental and theoretical cavity QED parameters for microsphere and Fabry-Perot cavities. ■ represents the current state of the art for cavity QED in Fabry-Perot cavities as in Ref. [30]. □ is a projection of the practical limit for Fabry-Perot cavities based upon Ref. [29]. ▲ represents the 60 μm radius sphere implemented for cavity QED in Ref. [31]. ▼ is the current state of the art in 10 μm microspheres based upon the results presented in Sec. VI. △ is the currently achievable Q with the optimal sphere size of 7.83 μm based upon the analysis of Secs. IV and V. ▽ is the theoretically achievable $Q \sim 9.76 \times 10^8$ at the optimal sphere size, $a \approx 7.83$ μm.

number $n_0 = 5.54 \times 10^{-3}$, and critical atom number $N_0 = 2.99 \times 10^{-2}$. If instead this experiment were to be implemented with a smaller sphere with 10 μm radius and with quality factor $Q \sim 0.8 \times 10^7$ such as we have manufactured and described in Sec. VI, the following parameters would be achieved: a mode volume of $V_{\vec{P}} \approx 1.4 \times 10^2$ μm^3, coupling coefficient $g_a/(2\pi) \approx 233$ MHz, saturation photon number $n_0 \approx 6.27 \times 10^{-5}$, and critical atom number $N_0 \approx 2.11 \times 10^{-3}$. Therefore, we see that currently achievable quality factors in spheres of radius 10 μm already would allow for impressive results in cavity QED with single atoms.

By comparison, the state of the art for Fabry-Perot cavities has already achieved the following results for the TEM_{00} modes [30]: a cavity finesse of $\mathcal{F} = 4.8 \times 10^5$, a mode volume of $V_m \approx 1.69 \times 10^3$ μm^3, coupling coefficient $g_0/(2\pi) \approx 110$ MHz, saturation photon number $n_0 \approx 2.82 \times 10^{-4}$, and critical atom number $N_0 \approx 6.13 \times 10^{-3}$. If one then looks at possible limits of Fabry-Perot technology for cavity QED as analyzed in Ref. [29], the following may be possible; a cavity of length $\lambda_0/2$ with a cavity finesse of $\mathcal{F} = 7.8 \times 10^6$ yields coupling coefficient $g_0/(2\pi) \approx 770$ MHz, saturation photon number $n_0 \approx 5.7 \times 10^{-6}$, and critical atom number $N_0 \approx 1.9 \times 10^{-4}$.

It is encouraging that the currently achievable results for small sphere manufacture would already allow the WGMs to compete favorably with the current state of the art in Fabry-Perot cavity QED. However, if one were able to manufacture and couple to spheres at the optimal size $a \approx 7.83$ μm with a $Q \sim 9.76 \times 10^8$ (the theoretical maximum predicted from the analysis of Sec. IV), the following results could be achieved: a mode volume of $V_{\vec{P}} \approx 90$ μm^3, coupling coefficient $g_a/(2\pi) \approx 318$ MHz, saturation photon number $n_0 \approx 3.36 \times 10^{-5}$, and critical atom number $N_0 \approx 9.28 \times 10^{-6}$. This would represent a significant improvement over the current Fabry-Perot technology and be competitive with the likely limits of Fabry-Perot technology. However, even short of achieving this stated maximum Q for the WGMs, impressive results can already be attained. With a quality factor $Q \sim 0.8 \times 10^7$ at the optimal sphere radius $a \approx 7.83$ μm, one would obtain these same results [i.e., $g_a/(2\pi) \approx 318$ MHz and saturation photon number $n_0 \approx 3.36 \times 10^{-5}$), except that the critical atom number N_0, would increase to $N_0 \approx 1.13 \times 10^{-3}$. This is still an impressive gain over the current capabilities of Fabry-Perot cavities for the saturation photon number, with room for improvement in the critical atom number.

Overall, we thus find that the technologies of microspheres and Fabry-Perot resonators each have their advantages and disadvantages. However, there is one notable advantage of microspheres; they can be made cheaply and relatively simply given sufficient training and skill. By contrast, the Fabry-Perot cavities considered here require specialized coating runs with expensive equipment and considerable expertise, which is to be found at only a few locations worldwide. This alone makes microspheres an attractive alternative to Fabry-Perot cavities for cavity QED. Another unique advantage of the WGMs is the ability to control the cavity decay rate κ by controlling the coupling efficiency into and out of the microsphere (e.g., by adjusting the distance between a coupling prism and the microsphere [32]). Furthermore, as one moves to the limit of small cavities, the open geometry of microspheres offers a considerable advantage when compared to the geometry of Fabry-Perot cavities. Such possibilities combined with our projected values of the critical parameters, (n_0, N_0), shown in Fig. 14 point to the competitiveness of microspheres with current and future Fabry-Perot technology and demonstrate their potential as a powerful tool for cavity QED in the regime of strong coupling.

ACKNOWLEDGMENTS

We thank K. Birnbaum, S. J. van Enk, C. Hood, V. Ilchenko, A. Kuzmich, R. Legere, P. Lodahl, T. Lynn, H. Mabuchi, J. McKeever, T. Northup, D. Vernooy, and J. Ye for helpful discussions. This work was supported by the National Science Foundation, by the Office of Naval Research, and by the Caltech MURI on Quantum Networks administered by the Office of Army Research.

[1] V.B. Braginsky and V.S. Ilchenko, [Sov. Phys. Dokl. **32**, 307 (1987)].
[2] M.L. Gorodetsky, A.A. Savchenkov, and V.S. Ilchenko, Opt. Lett. **21**, 453 (1995).
[3] D.W. Vernooy, V.S. Ilchenko, H. Mabuchi, E.W. Streed, and H.J. Kimble, Opt. Lett. **23**, 247 (1998).
[4] D.W. Vernooy and H.J. Kimble, Phys. Rev. A **55**, 1239 (1997).
[5] H. Mabuchi and H.J. Kimble, Opt. Lett. **19**, 749 (1994).
[6] M.L. Gorodetsky and V.S. Ilchenko, Opt. Commun. **113**, 133 (1994).
[7] F. Treussart, J. Hare, L. Collot, V. Lefèvre-Seguin, D.S. Weiss, V. Sandoghdar, J.M. Raimond, and S. Haroche, Opt. Lett. **19**, 1651 (1994).
[8] J.C. Knight, N. Dubreuil, V. Sandoghar, J. Hare, V. Lefèvre-Seguin, J.M. Raimond, and S. Haroche, Opt. Lett. **20**, 1515 (1995).
[9] J.C. Knight, N. Dubreuil, V. Sandoghar, J. Hare, V. Lefèvre-Seguin, J.M. Raimond, and S. Haroche, Opt. Lett. **21**, 698 (1996).
[10] W. Jhe and J.W. Kim, Phys. Rev. A **51**, 1150 (1995).
[11] H. Chew, J. Chem. Phys. **87**, 135 (1987).
[12] V.V. Klimov and V.S. Letokhov, Opt. Commun. **122**, 155 (1996).
[13] V.V. Klimov, M. Ducloy, and V.S. Letokhov, J. Mod. Opt. **43**, 549 (1996).
[14] W. Klitzing, R. Long, V.S. Ilchenko, J. Hare, and V. Lefèvre-Seguin, New J. Phys. **3**, 14 (2001).
[15] M.M. Mazumder, D.Q. Chowdhury, S.C. Hill, and R.K. Chang, *Optical Processes in Microcavities* (World Scientific, Singapore, 1996), Vol. 3.
[16] A.J. Campillo, J.D. Eversole, and H.-B. Lin, *Optical Processes in Microcavities*, Ref. [15].
[17] R.E. Slusher and U. Mohideen, *Optical Processes in Microcavities* (Ref. [15]).
[18] A.B. Matsko, S.P. Vyatchanin, H.J. Kimble, and H. Mabuchi, Phys. Lett. A **192**, 175 (1994).
[19] D.J. Norris, M. Kuwata-Gonokami, and W.E. Moerner, Appl. Phys. Lett. **71**, 297 (1997).
[20] X. Fan, A. Doran, and H. Wang, Appl. Phys. Lett. **73**, 3190 (1998).
[21] H.J. Kimble, *Cavity Quantum Electrodynamics* (Academic Press, San Diego, 1994).
[22] H.J. Kimble, Phys. Scr., T **T76**, 127 (1998).
[23] J.A. Stratton, *Electromagnetic Theory* (McGraw Hill, New York, 1997).
[24] Because the WGMs are the modes of an open resonator, the mode volume, $V_{\vec{P}}$, diverges as $r_Q \to \infty$. However, this divergence is logarithmic, and $V_{\vec{P}}$ is quite insensitive to the choice of r_Q for a large range of values. For example, at the optimal sphere size discussed in Sec. VI where $l=76$, $V_{\vec{P}}$ varies by less than 1% for $10<2\pi n/\lambda_0(r_Q-a)<10^3$. In this case, we take $(r_Q-a)\approx 100\ \mu$m.
[25] *Handbook of Optics*, 2nd ed., edited by M. Bass (McGraw Hill, New York, 1995), Vol. II, Chap. 33, p. 63.
[26] C. Lin, *Handbook of Microwave and Optical Components* (Wiley, New York, 1991).
[27] V.V. Datsyuk, Appl. Phys. B: Photophys. Laser Chem. **54**, 184 (1992).
[28] H.-B. Lin, J.D. Eversole, and A.J. Campillo, Opt. Commun. **77**, 407 (1990).
[29] C.J. Hood, J. Ye, and H.J. Kimble, Phys. Rev. A **64**, 033804 (2001).
[30] C.J. Hood, T.W. Lynn, A.C. Doherty, A.S. Parkins, and H.J. Kimble, Science **287**, 1457 (2000).
[31] D.W. Vernooy, A. Furusawa, N.P. Georgiades, V.S. Ilchenko, and H.J. Kimble, Phys. Rev. A **57**, R2293 (1998).
[32] M.L. Gorodetsky and V.S. Ilchenko, J. Opt. Soc. Am. B **16**, 147 (1999).